

https://dspace.org/

Multicolour emission from ZnOSO4Eu2 nanophosphors Effects of SO24 and Eu2 doping concentration

MLA Letswalo; L Reddy; A Balakrishna; MA Mamo; Rudolph Erasmus ...

https://hdl.handle.net/10539/40958
WOS

Downloaded from a DSpace repository. https://dspace.org/

Materials Today Communications 38 (2024) 107944

Contents lists available at ScienceDirect

Materials Today Communications

journal homepage: www.elsevier.com/locate/mtcomm

Multi-colour emission from $ZnO[SO_4]:Eu^{2+}$ nanophosphors: Effects of SO_4^{2-} and Eu^{2+} doping concentration

M.L.A. Letswalo [a,*], L. Reddy [a], A. Balakrishna [a,*], M.A. Mamo [b], R.M. Erasmus [c], O.M. Ntwaeaborwa [c,*]

[a] Department of Physics, University of Johannesburg, Johannesburg ZA2006, South Africa
[b] Department of Chemical Science, University of Johannesburg, Johannesburg ZA2006, South Africa
[c] School of Physics, University of the Witwatersrand, Johannesburg, WITS2050, South Africa

ARTICLE INFO

Keywords:
Solid-state reaction
Phosphors
Photoluminescence
Energy transfer

ABSTRACT

Blue-emitting $ZnO\text{-}SO_4:Eu^{2+}$ powder phosphors were synthesized via solid state reaction method. Based on the X-ray diffraction (XRD) data, hexagonal wurtzite structures of ZnO were formed. Further structural elucidation via Raman spectroscopy showed a peak at 439 cm^{-1} associated with E_{2hgh} optical mode that is a distinctive characteristic band of hexagonal wurtzite ZnO phase. The ZnO powders were composed of distorted spherical nanoparticles, which were agglomerated together as confirmed from scanning electron microscopy images. After incorporation of SO_4^{2-} and Eu^{2+} into the ZnO lattices sites, the particle shapes became irregular. When excited at 351 nm with Xenon lamp, our samples emitted UV and blue-green visible light associated, respectively, with excitonic recombination and intrinsic structural lattice defects in ZnO. Both the photoluminescence (PL) peak intensity and positions of these emissions were influenced by SO_4^{2-} and Eu^{2+} ions. The blue emission was dependent on the Eu^{2+} content with the largest intensity measured from the sample doped with 1.0 mol% of Eu^{2+} ions. Mechanisms of energy transfer and concentration quenching effect are discussed.

1. Introduction

ZnO is a semiconducting material that has been studied widely for application in lighting [1], gas sensors, solar cells and a wide variety of optoelectronic devices [2,3]. It is characterized by UV and visible light emission resulting from electron-hole recombination in the bandgap and intrinsic lattice defects, respectively. It has a bulk bandgap of 3.37 eV and the exciton binding energy of 60 meV [4], which is useful in optoelectronic devices. Although ZnO has a large and direct bandgap, it is highly capable of absorbing energy from the incident beam (e.g. photons) and generates photo excitations and emissions. In addition, ZnO is used as host for lanthanides and alkali earth ions to prepare phosphors that emits ultraviolet or visible or infrared light [5–7]. Doping of ZnO offers advantages such as: (1) tailoring of the bandgap by repositioning the conduction and valence bands, (2) enhancing absorbance, and (3) enhancing ZnO conductivity and charge carrier mobility. Many researchers have doped ZnO to increase charge traps, which reduce bulk recombination thereby allowing efficient separation of photogenerated electrons and holes [8–10]. Our earlier report showed significant improvement in green photoluminescence due to incorporation of sulphate ions in the zinc lattices sites [11].

In this paper, we report the effect of SO_4^{2-} on the blue photoluminescence of Eu^{2+} ions incorporated in ZnO crystal. Since Eu^{2+} is sensitive to the local crystal field of the host lattice compared to other popular dopant ions, its broad emission bands can be shifted across the visible spectrum. The blue emission was enhanced by a transfer of energy from $ZnO[SO_4]$ to Eu^{2+}. Energy transfer from the host lattices enhances photoemission intensity of rare-earths dopant ions that can in turn be used to improve performance and life span of light emitting diodes (LEDs), fluorescent lamps, fibre amplifiers and solid-state lasers [12–14]. Enhanced photoemission from different rare-earths ions because of phono-mediated transfer of energy from substitutional components has been reported. Ntwaeaborwa et al. [14] observed transfer of energy from ZnO to Ce^{3+} embedded in an amorphous glassy SiO_2 host. Dhlamini et al. [15] and Mhlongo et al. [16] have, respectively, demonstrated improved photoemission from Tb^{3+} and Pr^{3+} dopant ions because of transfer of energy from ZnO nanoparticles encapsulated in glassy SiO_2 host lattices. Usually, transfer of energy

* Corresponding authors.
E-mail addresses: letswalom@uj.ac.za (M.L.A. Letswalo), bavula@uj.ac.za (A. Balakrishna), martin.ntwaeaborwa@wits.ac.za (O.M. Ntwaeaborwa).

https://doi.org/10.1016/j.mtcomm.2023.107944
Received 18 October 2023; Received in revised form 8 December 2023; Accepted 20 December 2023
Available online 22 December 2023
2352-4928/© 2023 Elsevier Ltd. All rights reserved.

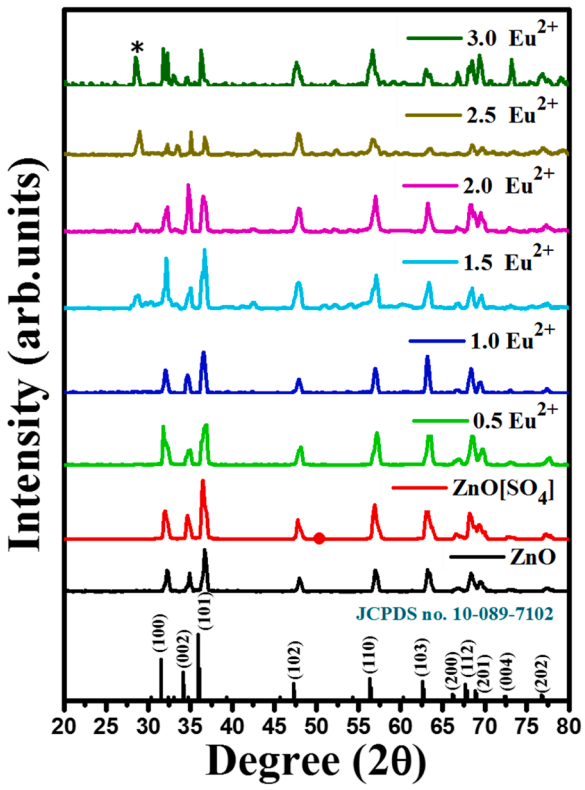

Fig. 1. X-ray diffraction spectra of undoped and SO_4^{2-} and (0.5 – 3 mol%) Eu^{2+} doped ZnO.

between ZnO and dopant ions takes place via primary excitation energy capture by intrinsic defect state of ZnO and subsequent transfer to the dopants and/or via free or bound excitonic state levels of ZnO. Balakrishna et al. [17] and Letswalo et al. [11] reported transfer of energy from substituted anionic groups such as BO_3^{3-}, PO_4^{3-} and SO_4^{3-} to Sm^{3+} and Eu^{3+} in molybdate hosts. The proposed energy transfer mechanisms between substituted groups and luminescent ions are speculative and therefore more research needs to be conducted to get a better understanding of these energy transfer mechanisms. Unlike most rare-earths dopant ions whose narrow emission bands are fixed because their 4 *f* orbitals are shielded from the local crystal field, the 4 *f* orbitals of Eu^{2+} are not shielded from the crystal field of the host lattice [18] and therefore their energy levels can be easily split, and the radiative transitions can be shifted. This makes Eu^{2+} an interesting dopant ion with exceptional luminescent properties and a wide range of applications. Eu^{2+} produces broad range of visible emissions in different host lattices

Table 1
Crystallographic data, structure Rietveld refinement parameters and particle size for ZnO, ZnO[SO_4] and ZnO[SO_4]:Eu^{2+} phosphors.

Sample Parameter	ZnO	ZnO[SO_4]	ZnO [SO_4]:1.0Eu^{2+}
Crystal phase	Hexagonal	Hexagonal	Hexagonal
Space group	P63mc	P63mc	P63mc
Lattice parameters (Å)	a = b = 3.2488c = 5.2054	a = b = 3.2539c = 5.20598	a = b = 3.2524c = 5.2162
R_p	2.73	2.52	4.25
R_{wp}	3.71	3.46	3.42
R_{exp}	2.72	2.51	4.39
Cell volume (Å^3)	47.58	47.77	47.60
Density (g/cm^3)	5.68	5.66	5.67
Particle size (nm) (Scherrer's method)	87	70	64

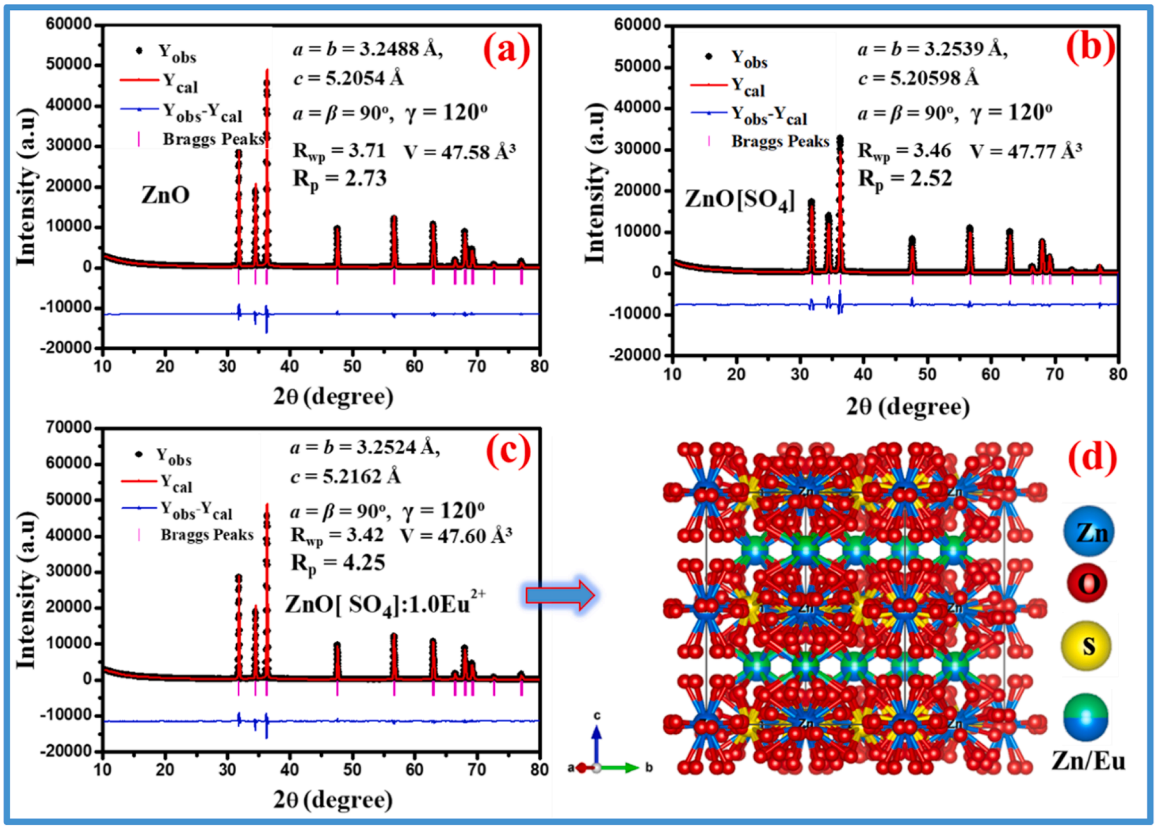

Fig. 2. (a) the Rietveld fits of (a) undoped, (b) SO_4^{2-} and (c) (1 mol%) Eu^{2+} doped ZnO crystal structures.

Table 2
Fractional atomic coordinates and occupancy factors for $ZnO[SO_4]:Eu^{2+}$ determined from the Rietveld refined structures.

Atom	x	y	z	Occupancy	Site
Zn1	0	0	0	1.000	2a
Zn2	0.5	0.5	0.5	1.000	6c
Zn3	0.99353	0.49885	0.24366	0.990	6c
Eu1	0.00648	0.50115	0.75634	0.010	6c
S1	0.87445	0.71945	0.51039	1.000	12d
S2	0.12555	0.28055	0.48961	1.000	12d
S3	0.77074	0.39625	0.01972	1.000	12d
S4	0.22926	0.60375	0.98028	1.000	12d
O1	0.00232	0.70692	0.62526	1.000	12d
O2	0.99768	0.29307	0.37474	1.000	12d
O3	0.95711	0.70571	0.3624	1.000	12d
O4	0.04289	0.29429	0.6376	1.000	12d
O5	0.74941	0.59459	0.54545	1.000	12d
O6	0.25059	0.40541	0.45455	1.000	12d
O7	0.8991	0.25293	0.04852	1.000	12d
O8	0.1009	0.74707	0.95148	1.000	12d

[18–22]. Red photoluminescence from Eu-doped ZnO nanostructures fabricated by microemulsion have been reported by various researchers [23–27]. Photoemission from Eu^{2+} ion is a result of electronic transition from excited 4 $f^6$5d energy states to 4 f^7 ground energy levels. Electron transition from the ground energy state (4 f^7 configuration) to the excited energy state (4 $f^6$5d configuration) is caused by absorption of primary excitation energy and emission results from electronic transition from the lowest energy band of the 4 f^6d configuration to the $^8S_{7/2}$ of the 4 f^7 configuration. Because of the higher spatial length of the 5d orbitals, the 4 $f^6$5d levels can be easily split by the crystal field compared to the 4 f^7 levels, and they are usually regarded as the metastable state, when the Eu^{2+} ion is incorporated in host lattices. The octahedral symmetry of the crystal field splits the 5d orbitals into two sub levels of $t_{2\ g}$ and e_g components [28,29].

We used soli-state reaction method to synthesize $ZnO[SO_4]:Eu^{2+}$ phosphors with different contents of Eu^{2+} and evaluated how SO_4^{2-} ions incorporated in ZnO host influenced defect emission from the host and the blue emission associated with the $5d \rightarrow 4f$ transitions of the Eu^{2+} ions. The mechanism of transfer of energy by phonon mediated process from ZnO and $ZnO[SO_4]$ to Eu^{2+} that enhanced the blue emission is proposed.

2. Experimental

2.1. Materials and synthesis

Solid-state reaction method was used to prepare ZnO, $ZnO[SO_4]$, and Eu^{2+} doped $ZnO[SO_4]$. Varying concentrations of Eu^{2+} from 0.5 to 3 mol % were added in constant increments of 0.5. The starting materials were high-purity grade ZnO (99.99%), $(NH_4)_2HSO_4$ (99.99%), and Eu_2O_3 (99.99%) powders. These materials were weighed stoichiometrically, mixed in acetone and ground for 45 min before sintering in a furnace in a reducing atmosphere (5%H_2/95%Ar) at 1000 °C for 6 h. After cooling the mixture to room temperature, the final products were ground gently using a pestle and mortar resulting in a fine powder.

2.2. Characterization techniques

The Bruker D8 Advanced X-ray diffractometer to conduct the X-ray diffraction analysis of the crystalline structure of the samples. A monochromatic source of radiation CuKα (λ = 0.15405 nm) was utilized, and measurements were taken within the range of 20 – 80° 2θ scans. Additionally, Nicolet Fourier transformed infrared (FTIR) spectrometry was used to examine the stretching frequency modes. The FE-SEM (field emission scanning electron microscope) and an energy dispersive spectrometer (EDS) were employed to study the particle morphology and elemental composition. The Raman scattering of ZnO was evaluated by analysing lattice vibrational modes using a Horiba Jobin-Yvon Raman Spectrometer. Furthermore, PL measurements were conducted using Horiba 800 spectrophotometer, at room temperature, equipped with a monochromatic Xenon lamp used as an excitation source. Finally, the UV–vis reflectance spectra were acquired using a Lambda 950 UV–Vis spectrometer.

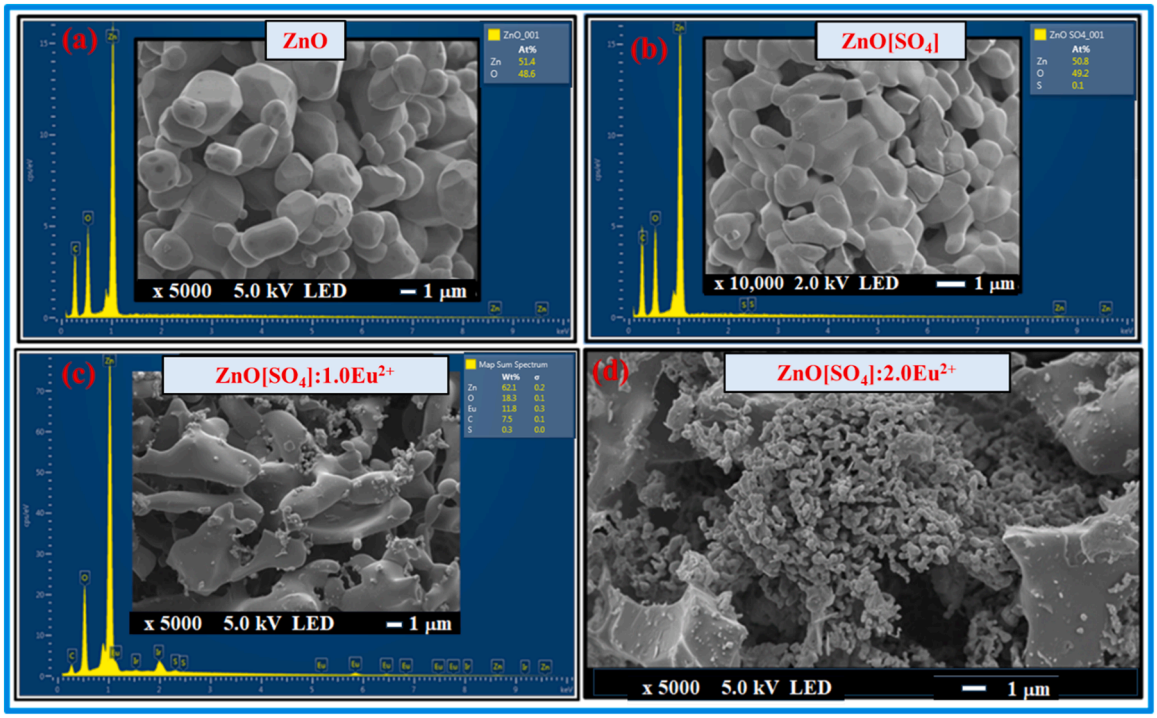

Fig. 3. (a-d) SEM images and (a-c) EDS spectra of ZnO, $ZnO[SO_4]$, and Eu^{2+}-doped $ZnO[SO_4]$ phosphors sintered in argon/hydrogen atmosphere. The insets are weight percentages of the elements.

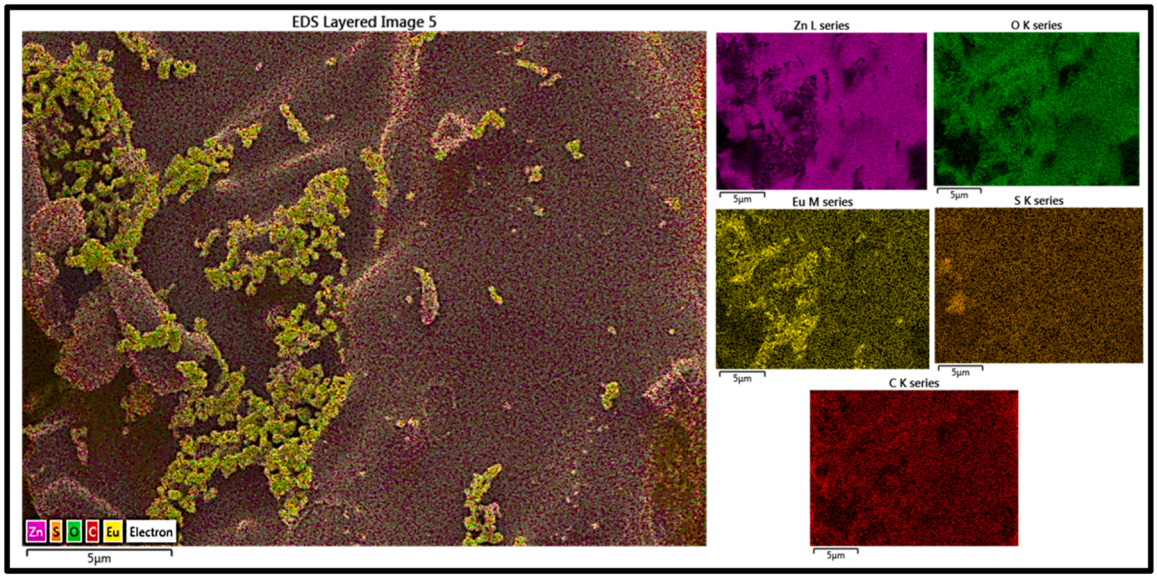

Fig. 4. EDS mapping of $ZnO[SO_4]$:1.0Eu^{2+} phosphor powder.

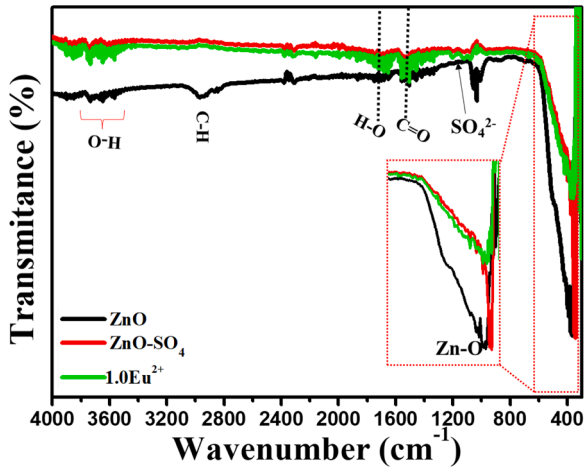

Fig. 5. FTIR spectra of undoped, SO_4^{2-} and (1 mol%) Eu^{2+} doped ZnO phosphors.

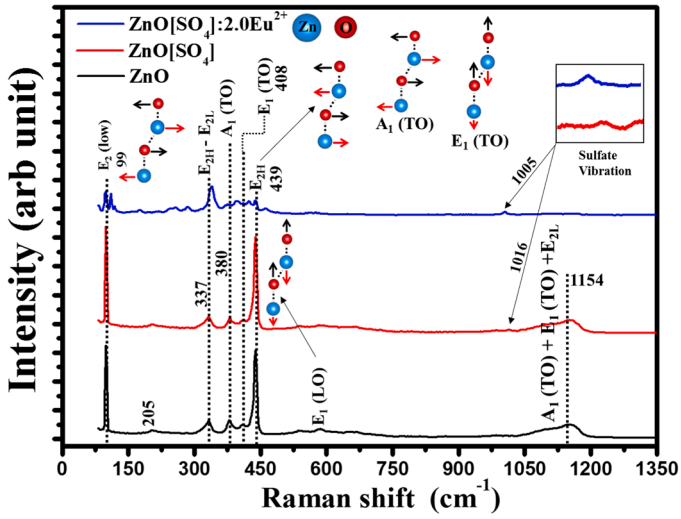

Fig. 6. Raman spectra of undoped, and SO_4^{2-} (2.0 mol%) and Eu^{2+}-doped ZnO phosphors.

3. Results and discussion

3.1. XRD powder diffraction analysis

The XRD spectra of the powder samples are displayed in Fig. 1. The diffraction peaks are the same of as those of a hexagonal ZnO phase referenced in JCPDS card number 01–080-0074 [30]. The crystal structure was not influenced by small amounts of SO_4^{2-} ions, suggesting that these ions were well dispersed in the host lattice. However, at larger concentrations (> 1.0 mol%) of Eu^{2+} a minor diffraction peak (marked with an asterisk (*)) was detected at 28.8° and was indexed to a secondary phase of Eu_2O_3 [31,32]. This peak can be attributed to incomplete decomposition of the precursor.

The crystal structures from the XRD data were refined using the Match and Full-Proof Rietveld refinement programme method and the results are presented in Fig. 2. The observed (black:colour online), calculated (red:colour online), and the difference (blue:colour online) XRD profiles of undoped and SO_4^{2-} and (1.0 mol%) Eu^{2+} doped ZnO are presented in Fig. 2(a)-(c) respectively. The structural parameters and the 5% reliability factors (R_{wp} and R_p) or simply R-factors were determined. The refined ZnO and SO_4^{2-} doped ZnO structures contain no impurities or secondary phases. Furthermore, no additional phases were detected in the 1.0 mol% Eu^{2+} doped $ZnO[SO_4]$ structure which is consistent with the Rietveld refinement results.

The crystallographic data and structural parameters obtained from the refinement are listed in Table 1. The results indicate that the basic hexagonal structure of ZnO was not affected by the substitutional ions SO_4^{2-} and Eu^{2+} ions and have the same space group P63mc. Additionally, the refinement R-values (R_p, R_{wp} and R_{exp}) were found to be in agreement with the hexagonal structure with the P63mc space group. The influence of adding SO_4^{2-} ions and Eu^{2+} ions was identified through the lattice parameters and cell volume of the unit cell structure. The results revealed that the lattice parameters and cell volume were slightly increased after adding SO_4^{2-} ions and Eu^{2+} ions. This ZnO lattice enlargement was related to the different ionic sizes of the Zn^{2+} (radius = 0.083 nm) and Eu^{2+} (radius = 0.117 nm) ions. Using the XRD data, Scherrer's method was employed to determine the crystalline sizes of the prepared nanophosphors. The calculated particle sizes are presented in Table 1. The results indicated that the variation of the particle sizes in the nanometre scale followed an increasing trend of ZnO>$ZnO[SO_4]$

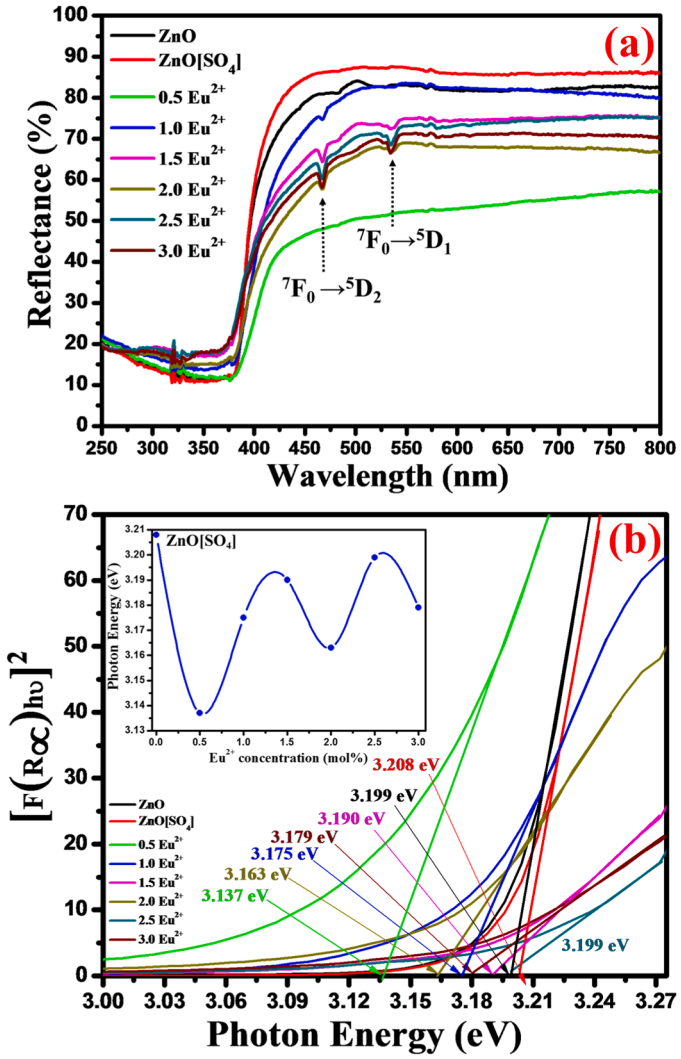

Fig. 7. (a) Diffuse reflectance spectra and the (b) Tauc plots from which the band gap energies were estimated.

> $ZnO[SO_4]$:1.0Eu^{2+} profile. The reduction in the crystalline size of the ZnO after substituting with SO_4^{2-} and Eu^{2+} ions is mainly attributed to the distortion of the ZnO lattice [33,34]. Table 2 displays the fractional atomic positions (x, y and z) and occupancy factors for $ZnO[SO_4]$:Eu^{2+} determined from the Rietveld refined structures.

3.2. Scanning electron microscopy analysis

The SEM images and EDS spectra of the powder samples are presented in Fig. 3(a)-(d). As observed from Fig. 3(a), ZnO is made up of distorted spheres. The degree of distortion increased upon incorporation of SO_4^{2-} (see Fig. 4(b). After incorporation of 1.0% and 2.0% of Eu^{2+}, there was a further increase in particle distortion giving rise to particles with irregular shapes (Fig. 3(c) and (d)). The EDS data confirmed all the elements present in the materials, together with their atomic weight percentages shown in the insets of Fig. 3(a), (b), and (c). Carbon (C) and Iridium (Ir) probably came from the carbon tape mountings and coating layers (used to prevent charging) respectively. The elemental mappings of $ZnO[SO_4]$:1.0Eu^{2+} powder are shown in Fig. 4. The mappings confirm an even distribution of Zn, S, O, Eu, and C elements.

3.3. Fourier transform infrared and Raman spectroscopy measurements

The Fourier transform infrared (FTIR) spectra of undoped and SO_4^{2-} and (1.0 mol%) Eu^{2+} doped ZnO are shown in Fig. 5. The well-known absorption band around 442 cm^{-1} in the spectra is attributed to stretching vibrations of Zn-O bonds [35,36]. The incorporation of sulphate compounds into the ZnO phosphors was confirmed by the peak located at 1206 cm^{-1}, which represented the SO_4^{2-} structural groups [37, 38]. The transmittance bands at 1648 cm^{-1} are assigned the C═O bonds, and those at 902 and 1375 cm^{-1} are due to the C-O bonds [37–39]. The C-H antisymmetric stretching bonds belong to a low signal peak at 2929 cm^{-1} [40–42]. The bands around 3609–3800 cm^{-1} are attributed to the O-H groups [43].

Raman spectra of ZnO, $ZnO[SO_4]$, and 2.0 mol% Eu^{2+}-doped ZnO $[SO_4]$ phosphors are shown in Fig. 6. The bands at 99, 337, 380, 408 and 439 cm^{-1} are assigned to wurtzite ZnO. The 439 cm^{-1} band is associated with the $E_{2\,H}$ mode of the non-polar optical phonons of ZnO. The bands at 327 and 380 cm^{-1} are associated with the A_1 symmetry (A1T) of ZnO nonpolar optical phonons in the $2E_{2\,L}$ and TO modes [44]. The peak at 205 cm^{-1} is due to lattice oxygen vacancies [45]. The enlarged portion of the spectra in the 1000–1025 cm^{-1} range, with major peaks at 1016 and 1005 cm^{-1}, is shown in the inset. These peaks possibly originated from the stretching vibrations of the sulphate anions [46]. The small band located at 584 cm^{-1} is attributed to E_1 symmetry for LO modes, which is due to lattice O-vacancies, Zn-interstitials, and free carriers [44,45]. Upon incorporation of Eu ions, the $E_{2\,H}$ Raman peak intensity decreases and there was a shift in the peak position from 437 cm^{-1} for ZnO to 439 cm^{-1} for the 2.0 mol% Eu^{2+}-doped $ZnO[SO_4]$ sample [45]. This confirms the successful substitution of Zn^{2+} ions by Eu^{2+} ions.

3.4. Diffuse reflectance spectroscopy

Fig. 7(a) and (b) show, respectively, the diffuse reflectance spectra (DRS) and Tauc plot of undoped, SO_4^{2-} and Eu^{2+} doped ZnO phosphors. All the DRS spectra exhibit prominent ZnO characteristic absorption edge in the range of 375 to 450 nm [47–52]. $ZnO[SO_4]$ has a relatively higher reflectance of 85% compared to all other samples, while the least reflection of~ 45% was recorded from $ZnO[SO_4]$:0.5 mol%Eu^{2+}. The weak absorption bands located at 466, and 525 nm are assigned to the $^7F_0 \rightarrow {}^5D_2$ and $^7F_0 \rightarrow {}^5D_1$ transitions of Eu^{3+} [53,54] respectively, which further confirms the presence of Eu_2O_3 as confirmed from the XRD data. The band gap energies were estimated from the Tauc plots in Fig. 7(b) [54]. The largest bandgap of 3.204 eV was determined from $ZnO[SO_4]$ and the narrowest bandgap of 3.137 eV was determined from 0.5% Eu-doped $ZnO[SO_4]$. The bandgap energies did not follow any particular trend but were rather fluctuating as the concentration of Eu^{2+} was varied from 0.5 to 3 mol%. This could be due to varying particles sizes, defect states, anion or cation vacancies, and interstitials (O_i/V_o) that don't occupy fixed positions in the bandgap of ZnO [55]. Again, it is most likely that the presence of Eu_2O_3 secondary phase (as confirmed from the XRD data) influenced the bandgap energy values.

3.5. Photoluminescence (PL) spectroscopy

Fig. 8(a) – (d) show the PL spectra measured when the powders where excited using a monochromatic Xenon lamp. Fig. 8(a) shows the spectra of undoped, and SO_4^{2-} and (1.0 mol%) Eu^{2+} doped ZnO. The major blue emission at 409 nm is associated with the $4f^6 5d^1 \rightarrow 4f^7$ transition of Eu^{2+} [51], while the broad emission bands peaking at 507 and 521 nm (Fig. 8(b)) are due to structural defects in ZnO. These bands also display small humps at 413 and 436 nm, which are associated with oxygen/zinc interstitials and oxygen/zinc vacancies. A marginal increase in the PL intensity and a slight red-shift of the spectrum were observed after incorporating SO_4^{2-} ions into the ZnO host. The observed changes are most probably due to transfer of energy, non-radiatively, between SO_4^{2-} and ZnO as illustrated in the deconvoluted PL emission spectra in Fig. 9(a) and (b). The photoemission spectra of ZnO-SO_4 with varying concentrations of Eu^{2+} are presented in Fig. 8(c). The highest

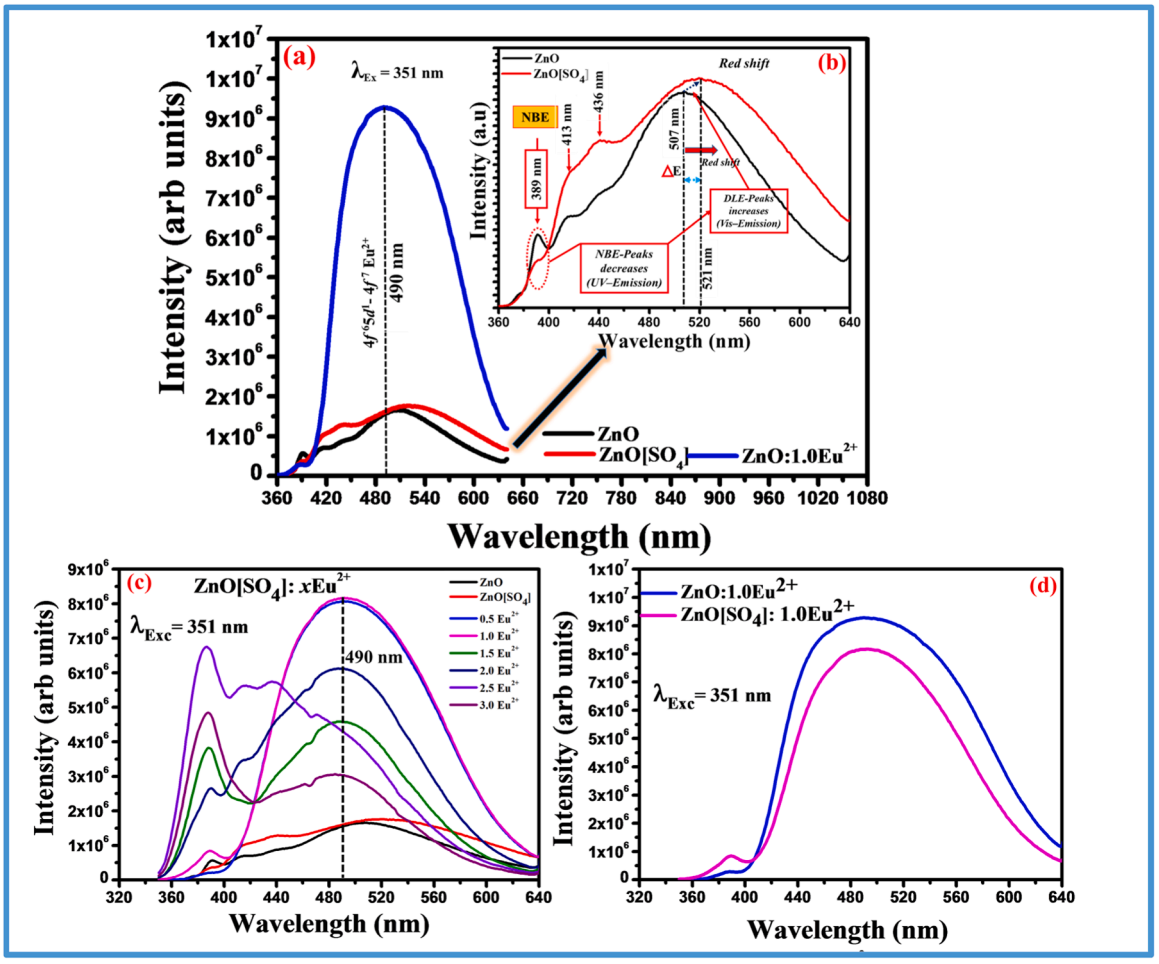

Fig. 8. PL spectra of (a) undoped, and SO_4^{2-} and 1 mol% Eu^{2+} doped ZnO, (b) ZnO[SO_4] and ZnO (enlarged), (c) ZnO[SO_4]: Eu^{2+} with varying content of Eu^{2+}, and (d) ZnO:Eu^{2+} (1 mol%) and ZnO[SO_4]:Eu^{2+} (1 mol%).

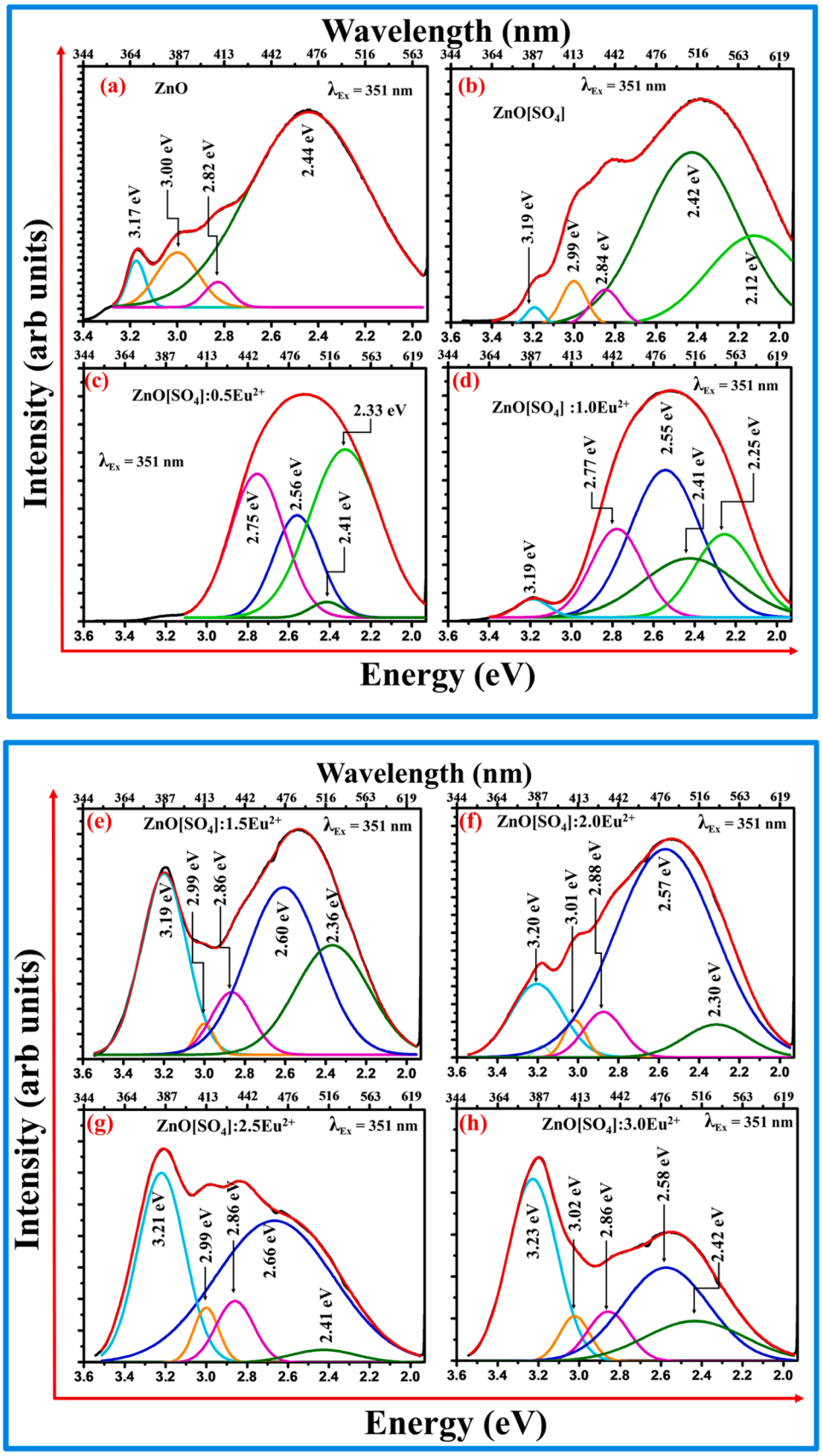

Fig. 9. (a)-(h): De-convoluted PL spectra of SO_4^{2-} and Eu^{2+} doped ZnO phosphors.

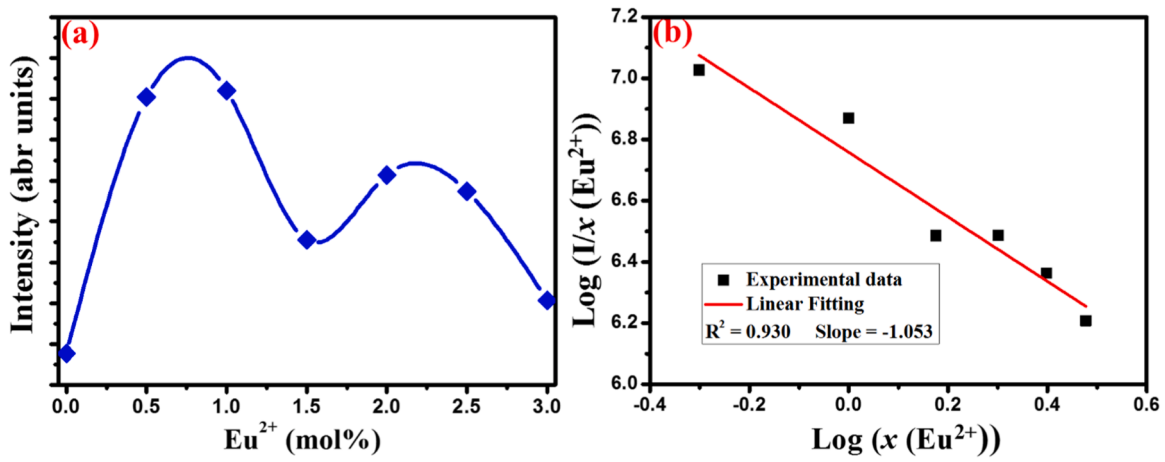

Fig. 10. (a) Intensity against Eu^{2+} concentration of $ZnO[SO_4]:xEu^{2+}$ (0–3.0 mol%) and (b)Linear fitting of log (x (Eu^{2+})) against log (I/ x (Eu^{2+})) with different Eu^{2+} concentration for $ZnO[SO_4]:Eu^{2+}$ phosphors.

photoemission was observed from the 0.5 and 1 mol% of Eu^{2+} doping. The peak position for these two spectra is located at 490 nm, confirming that the emissions are attributable to the 4 $f^6 5d^1 \rightarrow 4f^7$ transitions of the Eu^{2+}dopant ions. The PL peak intensity decreased with increasing Eu^{2+} dopant concentrations. The decrease of PL intensity with increasing Eu^{2+} dopant concentration is attributed to effects of concentration quenching. In addition, there is a relative increase in the well-known UV emission at ~ 389 nm, which is attributed to band-to-band transition in ZnO. The ~ 389 nm emission is maximum for 2.5 mol% of Eu^{2+} doping, and the main emission peak is blue-shifted from 490 nm, which is indicative of the changes in radiative transitions. This blue-shifted emission is associated with intrinsic defects in $ZnO[SO_4]$ [52,53].

The quenching of photoluminescence at 490 nm with increasing concentration of Eu^{2+} is known to occur via cross-relaxation processes between two identical centres. The decrease in the PL intensity was noticeable when the concentration of Eu^{2+} exceeded 1.0 mol%. To evaluate the concentration quenching effect of the $ZnO[SO_4]:xEu^{2+}$ phosphors, the critical distance R_c between identical Eu^{2+} ions was calculated using the following formula proposed by Blasse [54]:

$$R_c = 2\left(\frac{3V}{4\pi C_0 N}\right)^{\frac{1}{3}} \quad (1)$$

where N is the number of ions per unit cell, V is the volume of the unit cell, C_0 is the ideal activator (Eu^{2+}) concentration. Using $N = 1.0$, $C_0 = 0.01$, and V = 47.77 Å, the R_c value for Eu^{2+} ions were found to be 20.89 Å [55]. This value is greater than 5 Å, pointing to lack of transfer of energy between Eu^{2+} ions in the ZnO-SO_4 host. It shows that non-radiative transfer of energy was not possible at higher concentrations of Eu^{2+} ions in this electric multipolar interaction and this contributed to the quenching of luminescence from Eu^{2+}. Fig. 8(d) compares the photo-emission spectra of $ZnO:Eu^{2+}$ (1 mol%) to that of $ZnO[SO_4]:Eu^{2+}$ (1 mol%). For the same molar concentration of Eu^{2+}, the PL emission from $ZnO:Eu^{2+}$ is more intense than that of $ZnO[SO_4]:Eu^{2+}$, suggesting that the transfer rate of primary excitation energy from ZnO to Eu^{2+} was faster and more efficient compared to the transfer rate from $ZnO[SO_4]$ to Eu^{2+}.

Deconvoluted PL spectra of the powder phosphors are shown in Fig. 9(a)-(h) The emission bands at ~ 392 – 383 nm [~3.17 - 3.23 eV] in Fig. 9(a) are attributed to band-to-band recombination in ZnO. The blue emission band at ~ 414 – 436 nm [~2.99 – 2.84 eV] in Fig. 9(b) are assigned to zinc vacancies (V_{Zn}), while those at ~ 513 – 584 nm [~ 2.77 - 2.12 eV] are due to electronic transitions from the conduction band/zinc interstitial states to zinc vacancy. The major blue emission bands in Fig. 9(c)-(d) at ~ 2.56 eV are attributed to 4 $f^6 5d^1$- 4 $f^7 Eu^{2+}$ transitions. The emission bands in Fig. 9(e)-(h) are associated with intrinsic defects, i.e. transition from the conduction band to oxygen vacancy (V_o^+)/zinc vacancy/electronic transition from zinc interstitial (Zn_i) to oxygen interstitial (O_i) [56,57]. The blue emission bands in Fig. 9(c)-(d) are shifting with varying concentration of Eu^{2+}. Studies conducted by H. Sugimoto et al. [51] reported similar emission bands [52,53,58].

From Fig. 9(a)-(h), the emission peaks associated with various defect levels such as the green emission located at 512 nm (2.42 eV) in 0.5 and 1.0 mol% Eu^{2+} doped $ZnO[SO_4]$ phosphor are less intense than those observed in the undoped ZnO (Fig. 9(a)). This energy loss in ZnO emission centres is probably due to incorporation of Eu^{2+} ions to which energy was transferred from the Zn-O anti-bonding orbitals [54,59].

A further analysis of the decrease in the blue emission with increasing doping concentration of Eu^{2+} was performed using the Dexter formula [60–63]:

$$I/x = k[1 + \beta(x)^{\frac{\theta}{3}} \quad]^{-1} \quad (2)$$

where I is the emission intensity, x is the activator concentration, k and β are the host constants under the same excitation conditions and θ is the electric multipolar character. As shown in Fig. 10 (a), a double-logarithmic graph of log (I/x) as a function of log (x) was constructed to determine the value of θ, and the relationship between these is displayed in Fig. 10 (b). For $\theta = 6$, 8, and 10, the multipolar interactions for transfer of energy are dipole-dipole, dipole-quadrupole and quadrupole-quadrupole, respectively [61]. The slope ($\frac{\theta}{3}$) of log (I/x) as a function of log (x) curve was calculated to be –1.681, from which the value of θ was found to be 5.04, which is very close to 6. The interaction that is assigned to the value of $\theta = \sim 6$ is dipole-electric dipole. This further confirms that the concentration quenching in Eu^{2+} doped $ZnO[SO_4]$ nanophosphors was a result of electric dipole-electric dipole interactions.

The proposed simplified energy level diagrams of energy transfer mechanisms in our samples are depicted in Fig. 11 (a-c). Fig. 11 (a) shows the simplified energy level diagram of ZnO phosphor, which describes the possible electronic transitions extracted from deconvoluted PL spectra of ZnO. The defect emission band located at 391 nm (3.17 eV) is related to the electron-hole recombination in the bandgap of ZnO. The other emission bands centred at 414 nm (2.99 eV) and (439 nm) 2.82 eV are attributed to zinc vacancies V_{Zn}, and zinc interstitials (Zn_i) respectively. The deconvoluted broad band centred at 530 nm (~2.44 eV) is related to singly ionized V_o^+ oxygen vacancy. Similar transitions were observed in $ZnO[SO_4]$ (Fig. 11 (b)), except for the emission peak at 584 nm (~2.12 eV), which is assigned to oxygen interstitials (O_i). Fig. 11 (c) shows a simplified energy level diagram of ZnO demonstrating energy transfer mechanism from ZnO host to Eu^{2+}. The primary excitation energy was captured by ZnO followed by excited electrons

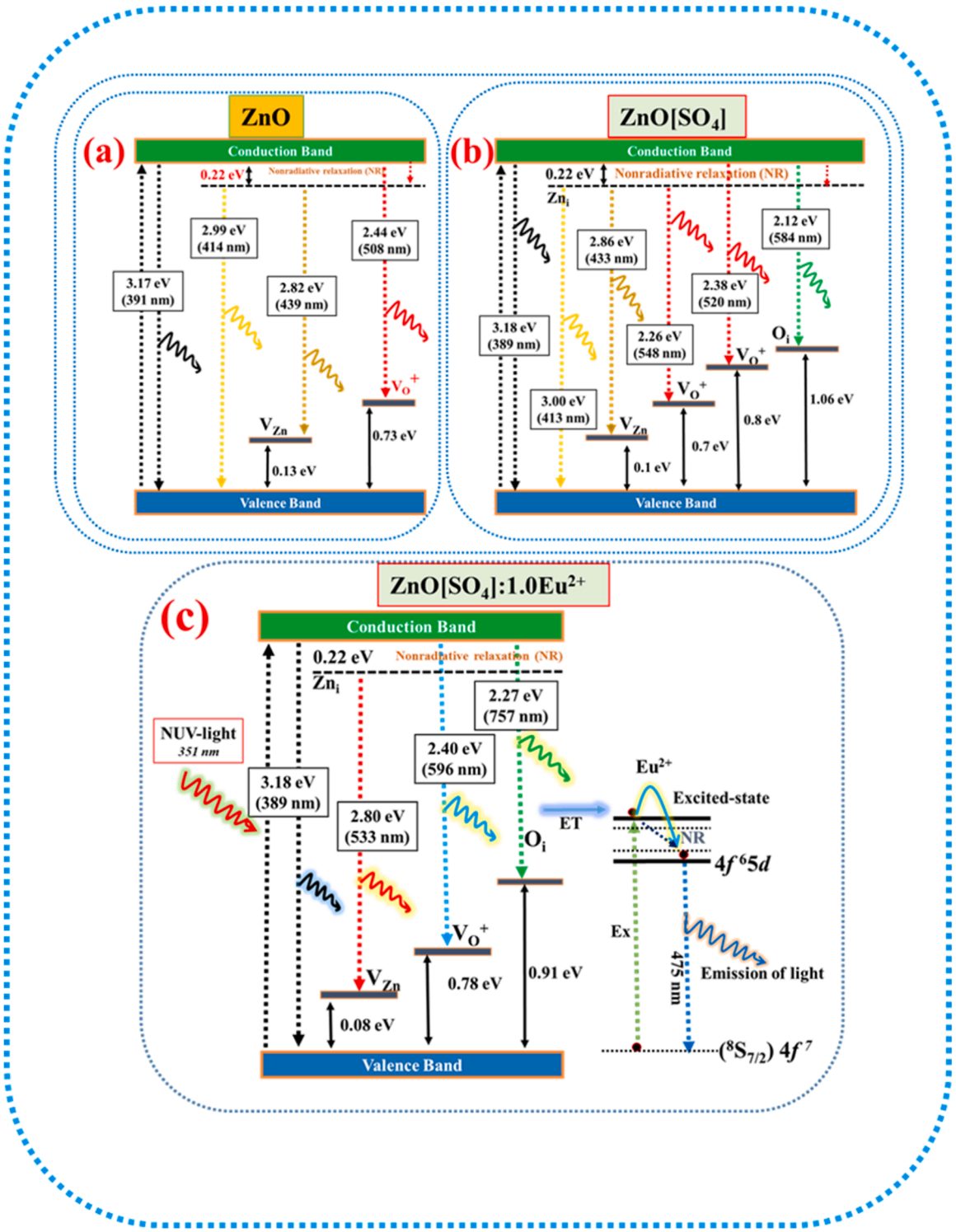

Fig. 11. Simplified energy level diagrams of light emission mechanisms based on deconvoluted PL emission spectrum of (a) ZnO, (b) $ZnO[SO_4]$, and (c) $ZnO[SO_4]:1.0Eu^{2+}$.

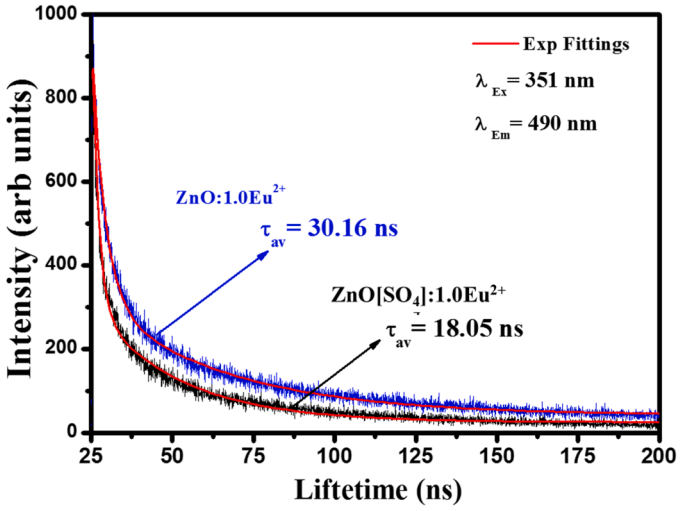

Fig. 12. The decay curves for $ZnO[SO_4]:0.5Eu^{2+}$ and $ZnO[SO_4]:1.0Eu^{2+}$ phosphors.

Table 3
Undoped ZnO, $ZnO[SO_4]$ and $ZnO[SO_4]:xEu^{2+}$ and CCT values and the correlating colours are coordinated by CIE1931 chromaticity.

Sample	CIE 1931 Coordinates *x y*		CCT (K)	Color
ZnO	0.33	0.36	5596	White
$ZnO[SO_4]$	0.32	0.36	6007	White
$ZnO:1.0:Eu^{2+}$	0.26	0.35	9235	Bluish-Green
$ZnO[SO_4]:0.5Eu^{2+}$	0.24	0.34	10985	Bluish-Green
$ZnO[SO_4]:1.0Eu^{2+}$	0.24	0.35	10568	Bluish-Green
$ZnO[SO_4]:1.5Eu^{2+}$	0.24	0.30	13610	Greenish-blue
$ZnO[SO_4]:2.0Eu^{2+}$	0.23	0.30	14829	Greenish-blue
$ZnO[SO_4]:2.5Eu^{2+}$	0.21	0.21	18761	Dark-Blue
$ZnO[SO_4]:3.0Eu^{2+}$	0.23	0.27	19890	Blue

moving from Zn-O anti-bonding orbitals to similar orbitals in Eu^{2+} with a subsequent radiative relaxation to the ground state. Energy transfer probably took place by phonon mediated processes.

Furthermore, we recorded the luminescence decay curves of ZnO: xEu^{2+} ($x = 1.0$ mol%) and $ZnO[SO_4]:xEu^{2+}$ ($x = 1.0$ mol%) phosphors excited at 351 nm while monitoring the 490 nm emission at room temperature (see Fig. 12). These lifetime decay curves were fitted with double-exponential function [64]. The average lifetime values of $ZnO:1.0Eu^{2+}$ and $ZnO[SO_4]:1.0Eu^{2+}$ were found to be 30.16 and 18.91 ns, respectively. This result confirms that the transfer rate of captured primary excitation energy to Eu^{2+} from ZnO was faster and more efficient than that from $ZnO[SO_4]$ to Eu^{2+}.

3.6. Commission International de l'Eclairage (CIE) and correlated colour temperature (CCT)

The CIE (*x, y*) colour coordinates of ZnO, $ZnO[SO_4]$ and a series of $ZnO[SO_4]:xEu^{2+}$ with different concentrations of Eu^{2+} ion were evaluated, and are presented in Table 3. The schematic CIE diagram is displayed in Fig. 13. It shows that the emission colours were tuneable from blue to white to bluish-green in the visible region. ZnO and $ZnO[SO_4]$ produced white light with colour coordinates (0.33,0.36) and (0.32,0.36) respectively. In general, Eu^{2+} doping produced tuneable blue to bluish-green emission associated with the $5d \rightarrow 4f$ transition of Eu^{2+}ions. This tunability was dependent on the Eu^{2+} concentration. In addition, the correlated colour temperature (CCT) of the synthesized materials was influenced by SO_4 and Eu^{2+} doping, and day-white-light to blue-skylight were attained as the Eu concentration was varied. These results indicate that our materials can be useful in colour display applications.

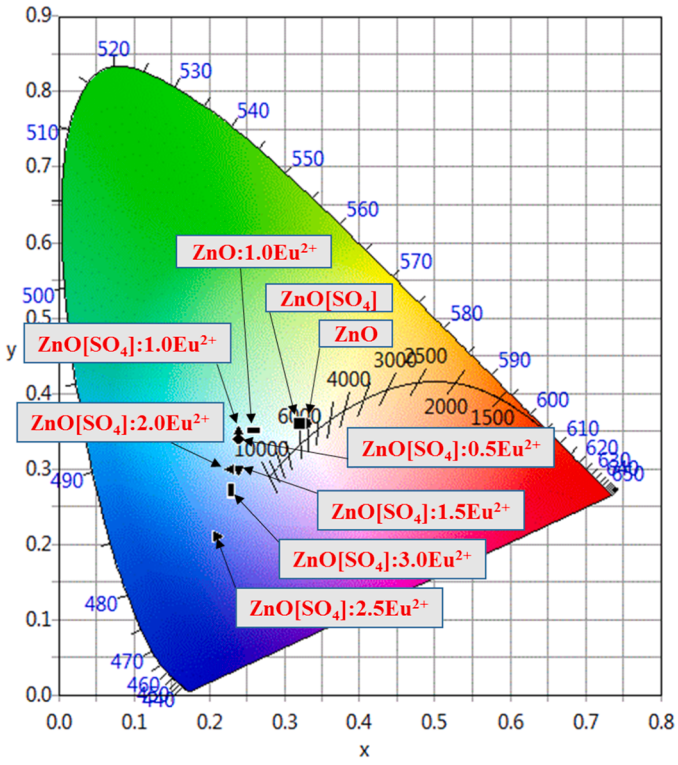

Fig. 13. (a) Schematic configuration coordinate diagram for $ZnO[SO_4]:xEu^{2+}$ and (b) ZnO, $ZnO[SO_4]$, $ZnO:1.0Eu^{2+}$ and $ZnO[SO_4]:xEu^{2+}$ (where x = 0.5-3.0) phosphors CIE chromaticity diagram.

4. Conclusions

We successfully prepared $ZnO[SO_4]:Eu^{2+}$ nanophosphors via high temperature solid state reaction method. We investigated the optical and photoluminescence properties of $ZnO[SO_4]:Eu^{2+}$ nanophosphors. Upon excitation at 351 nm, ZnO and $ZnO[SO_4]$ nanophosphors exhibited emission bands in the UV and visible regions. These broad emission bands were associated with excitonic recombination and native defects in ZnO. However the $ZnO[SO_4]:Eu^{2+}$ nanophosphors exhibited one more additional blue emission peak at 495 nm, which was ascribed to the $5d$-$4f$ transitions of Eu^{2+} ions. The luminescent decay curves suggested that energy transfer took place from the host lattices to Eu^{2+} dopants. This was also confirmed through dipole–dipole interaction theoretical calculations. The calculated colour coordinates indicated that the Eu^{2+} emission lay in the blue colour region of the CIE diagram. From all the results, we concluded that the prepared $ZnO[SO_4]:Eu^{2+}$ phosphors was showing colour tuneable behaviour which can play a crucial role in white LED and NUV LED applications.

Ethical Procedure

The research meets all applicable standards with regard to the ethics of experimentation and research integrity, and the following is being certified/declared true. As an expert scientist and along with co-authors of concerned field, the paper has been submitted with full responsibility, following due ethical procedure, and there is no duplicate publication, fraud, plagiarism, or concerns about animal or human experimentation.

Conflict of interest

None of the authors of this paper has a financial or personal relationship with other people or organizations that could inappropriately influence or bias the content of the paper. It is to specifically state that "No Competing interests are at stake and there is No Conflict of Interest"

with other people or organizations that could inappropriately influence or bias the content of the paper.

Declaration of Competing Interest

The authors declare that they have no known competing financial interests or personal relationships that could have appeared to influence the work reported in this paper.

Data Availability

Data will be made available on request.

References

[1] Z. Shi, Y. Zhang, X. Cui, S. Zhuang, B. Wu, X. Chu, X. Dong, B. Zhang, G. Du, Photoluminescence performance enhancement of ZnO/MgO heterostructured nanowires and their applications in ultraviolet laser diodes, Phys. Chem. Chem. Phys. vol. 17 (21) (2015) 13813–13820, https://doi.org/10.1039/c5cp00674k.

[2] E. Magnusson, B. Williams, R. Manenti, M. Nam, A. Nersisyan, M. Peterer, A. Ardavan, P. Leek, Surface acoustic wave devices on bulk ZnO crystals at low temperature, Appl. Phys. Lett. vol. 106 (6) (2015) 063509, https://doi.org/10.1063/1.4908248.

[3] O. Klutha, Editorial, Thin Solid Films vol. 351 (1-2) (1999) XIII, https://doi.org/10.1016/s0040-6090(99)00463-0.

[4] A. Tsukazaki, M. Kubota, A. Ohtomo, T. Onuma, K. Ohtani, H. Ohno, S.F. Chichibu, M. Kawasaki, Blue light-emitting diode based on ZnO, Jpn. J. Appl. Phys. vol. 44 (21) (2005) L643–L645, https://doi.org/10.1143/jjap.44.l643.

[5] W. Jia, K. Monge, F. Fernandez, Energy transfer from the host to Eu^{3+} in ZnO, Opt. Mater. vol. 23 (1-2) (2003) 27–32, https://doi.org/10.1016/s0925-3467(03)00054-5.

[6] C. Yang, S. Cheng, H. Lee, S. Chen, Effects of phase transformation on photoluminescence behavior of ZnO:Eu prepared in different solvents, Ceram. Int. vol. 32 (1) (2006) 37–41, https://doi.org/10.1016/j.ceramint.2004.11.016.

[7] P. Che, J. Meng, L. Guo, Oriented growth and luminescence of ZnO:Eu films prepared by sol–gel process, J. Lumin. vol. 122-123 (2007) 168–171, https://doi.org/10.1016/j.jlumin.2006.01.076.

[8] X. Kang, S. Liu, Z. Dai, Y. He, X. Song, Z. Tan, Titanium dioxide: from engineering to applications, Catalysts vol. 9 (2) (2019) 191, https://doi.org/10.3390/catal9020191.

[9] B. Pant, M. Park, H. Kim, S. Park, Ag-ZnO photocatalyst anchored on carbon nanofibers: synthesis, characterization, and photocatalytic activities, Synth. Met. vol. 220 (2016) 533–537, https://doi.org/10.1016/j.synthmet.2016.07.027.

[10] S. Singhal, S. Dixit, A. Shukla, Self-assembly of the Ag deposited ZnO/carbon nanospheres: a resourceful photocatalyst for efficient photocatalytic degradation of methylene blue dye in water, Adv. Powder Technol. vol. 29 (12) (2018) 3483–3492, https://doi.org/10.1016/j.apt.2018.09.031.

[11] M.L.A. Letswalo, L. Reddy, A. Balakrishna, H.C. Swart, O.M. Ntwaeaborwa, The role of sulfate ions on distinctive defect emissions in ZnO:Ce^{3+} nanophosphors - a study on the application in color display systems, J. Lumin. vol. 240 (2021) 118462, https://doi.org/10.1016/j.jlumin.2021.118462.

[12] S. Ashtaputre, A. Nojima, S. Marathe, D. Matsumura, T. Ohta, R. Tiwari, G. Dey, S. Kulkarni, Investigations of white light emitting europium doped zinc oxide nanoparticles, J. Phys. D: Appl. Phys. vol. 41 (1) (2007) 015301, https://doi.org/10.1088/0022-3727/41/1/015301.

[13] M. Ihara, T. Igarashi, T. Kusunoki, K. Ohno, 49.3: Preparation and characterization of rare earth activators doped nanocrystal phosphors, SID Symp. . Dig. Tech. Pap. vol. 30 (1) (1999) 1026, https://doi.org/10.1889/1.1833941.

[14] O.M. Ntwaeaborwa, P.H. Holloway, Enhanced photoluminescence of Ce^{3+}induced by an energy transfer from ZnO nanoparticles encapsulated in SiO_2, Nanotechnology vol. 16 (6) (2005) 865–868, https://doi.org/10.1088/0957-4484/16/6/042.

[15] M.S. Dhlamini, O.M. Ntwaeaborwa, H.C. Swart, J.M. Ngaruiya, K.T. Hillie, Sensitized luminescence through nanoscopic effects of ZnO encapsulated in SiO_2: Tb^{3+} sol gel derived phosphor, Phys. B: Condens. Matter vol. 404 (22) (2009) 4406–4410, https://doi.org/10.1016/j.physb.2009.09.045.

[16] G.H. Mhlongo, O.M. Ntwaeaborwa, H.C. Swart, R.E. Kroon, R. Solarz, P. Ryba-Romanowski, W, K.T. Hillie, Luminescence dependence of Pr^{3+} activated SiO_2 nanophosphor on Pr^{3+} concentration, temperature, and ZnO incorporation, J. Phys. Chem. C. 115 (36) (2011) 17625–17632.

[17] A. Balakrishna, H.C. Swart, R. Ramaraghavulu, A. Bedyal, R. Kroon, O. M. Ntwaeaborwa, Structural evolution induced by substitution of designated molybdate sites (MoO_4^{2-}) with different anionic groups (BO_3^{3-}, PO_4^{3-} and SO_4^{2-}) in $CaMoO_4$:Sm^{3+} phosphors-a study on color tunable luminescent properties, J. Alloy. Compd. vol. 727 (2017) 224–237, https://doi.org/10.1016/j.jallcom.2017.08.117.

[18] Z. Xia, Y. Zhang, M. Molokeev, V. Atuchin, Y. Luo, Linear structural evolution induced tunable photoluminescence in clinopyroxene solid-solution phosphors, Sci. Rep. vol. 3 (1) (2013), https://doi.org/10.1038/srep03310.

[19] G. Li, Y. Tian, Y. Zhao, J. Lin, Recent progress in luminescence tuning of Ce^{3+} and Eu^{2+} activated phosphors for pc-WLEDs, Chem. Soc. Rev. vol. 44 (23) (2015) 8688–8713, https://doi.org/10.1039/c4cs00446a.

[20] L. Lin, L. Ning, R. Zhou, C. Jiang, M. Peng, Y. Huang, J. Chen, Y. Huang, Y. Tao, H. B. Liang, Site occupation of Eu^{2+} in $Ba_{2-x}Sr_xSiO_4$ (x = 0–1.9) and origin of improved luminescence thermal stability in the intermediate composition, Inorg. Chem. vol. 57 (12) (2018) 7090–7096, https://doi.org/10.1021/acs.inorgchem.8b00773.

[21] D. Hou, C. Liu, X. Ding, X. Kuang, H. Liang, S. Sun, Y. Huang, Y. Tao, A high efficiency blue phosphor $BaCa_2MgSi_2O_8$:Eu^{2+} under VUV and UV excitation, J. Mater. Chem. C. vol. 1 (3) (2013) 493–499, https://doi.org/10.1039/c2tc00129b.

[22] H. Ji, Z. Huang, Z. Xia, M. Molokeev, V. Atuchin, S. Huang, Cation substitution dependent bimodal photoluminescence in whitlockite structural $Ca_{3-x}Sr_x(PO_4)_2$: Eu^{2+} ($0 \leq x \leq 2$) solid solution phosphors, Inorg. Chem. vol. 53 (20) (2014) 11119–11124, https://doi.org/10.1021/ic501679f.

[23] R. Bhargava, V. Chhabra, T. Som, A. Ekimov and N. Taskar, Quantum Confined Atoms of Doped ZnO Nanocrystals, physica status solidi (b), vol. 229, no. 2, pp. 897–901, 2002. Available: 10.1002/1521–3951(200201)229:2<897::aid-pssb897>3.0.co;2-c.

[24] A. Ishizumi, Y. Kanemitsu, Structural and luminescence properties of Eu-doped ZnO nanorods fabricated by a microemulsion method, Appl. Phys. Lett. vol. 86 (25) (2005) 253106, https://doi.org/10.1063/1.1952576.

[25] S. Sadhu, T. Sen, A. Patra, Shape controlled synthesis and luminescence properties of ZnO: Eu^{3+} nanostructures, Chem. Phys. Lett. vol. 440 (1-3) (2007) 121–124, https://doi.org/10.1016/j.cplett.2007.04.015.

[26] S. Lima, M. Davolos, W. Quirino, C. Legnani, M. Cremona, Low-voltage electroluminescence of europium in zinc oxide thin films, Appl. Phys. Lett. vol. 90 (2) (2007) 023503, https://doi.org/10.1063/1.2431566.

[27] S. Gao, H. Zhang, R. Deng, X. Wang, D. Sun, G. Zheng, Engineering white light-emitting Eu-doped ZnO urchins by biopolymer-assisted hydrothermal method, Appl. Phys. Lett. vol. 89 (12) (2006) 123125, https://doi.org/10.1063/1.2357031.

[28] D. Gahane, N. Kokode, B. Bahirwar, S. Moharil, Luminescence of Eu^{2+} in some chlorides, Phys. Procedia vol. 29 (2012) 42–45, https://doi.org/10.1016/j.phpro.2012.03.689.

[29] J. Chen, Y. Liu, H. Liu, H. Ding, M. Fang, Z. Huang, Tunable $SrAl_2Si_2O_8$: Eu phosphor prepared in air via valence state-controlled means, Opt. Mater. vol. 42 (2015) 80–86, https://doi.org/10.1016/j.optmat.2014.12.023.

[30] Calculated from ICSD using POWD-12++, (1997) Garcia-Martinez, O., Rojas, R.M., Vila, E., Martin de Vidales, J.L., Solid State Ionics, Vol. 63, pp. 442, 1993.

[31] W. Mohamed, A. Abu-Dief, Synthesis, characterization and photocatalysis enhancement of Eu_2O_3-ZnO mixed oxide nanoparticles, J. Phys. Chem. Solids vol. 116 (2018) 375–385, https://doi.org/10.1016/j.jpcs.2018.02.008.

[32] L. Koao, B. Dejene, H. Swart, S. Motloung, T. Motaung, Characterization of annealed Eu^{3+} -doped ZnO flower-like morphology synthesized by chemical bath deposition method, Opt. Mater. vol. 60 (2016) 294–304, https://doi.org/10.1016/j.optmat.2016.07.042.

[33] M. Sajjad, I. Ullah, M.I. Khan, J. Khan, M.Y. Khan, M.T. Qureshi, Structural and optical properties of pure and copper doped zinc oxide nanoparticles, Results Phys. 9 (2018) 1301–1309.

[34] G. Vijayaprasath, R. Murugan, S. Asaithambi, G.Anandha Babu, P. Sakthivel, T. Mahalingam, Y. Hayakawa, G. Ravi, Structural characterization and magnetic properties of Co co-doped Ni/ZnO nanoparticles, Appl. Phys. A 122 (2016) 122, https://doi.org/10.1007/s00339-016-9655-0.

[35] S.J. Jun, S. Kim, J.H. Han, Synthesis of stoichiometric hydroxyapatite powder by CO_3^{2-}substitution during precipitation, J. Korean Ceram. Soc. Vol. 35 (No.3) (1998) 209–213.

[36] Y.J. Kwon, K.H. Kim, C.S. Lim, K.B. Shim, Characterization of ZnO nanopowders synthesized by the polymerized complex method via an organochemical route, J. Ceram. Process. Res. Vol. 3 (2002) 146–149.

[37] S. Jung, P. Grange, Characterization and reactivity of pure TiO_2–SO_4^{2-} SCR catalyst: influence of SO_4^{2-} content, Catal. Today vol. 59 (3-4) (2000) 305–312, https://doi.org/10.1016/s0920-5861(00)00296-0.

[38] D. Guan, M. Fan, J. Wang, Y. Zhang, Q. Liu, X. Jing, Synthesis and properties of magnetic solid superacid: SO_4^{2-}/ZrO_2–B_2O_3–Fe_3O_4, Mater. Chem. Phys. vol. 122 (1) (2010) 278–283, https://doi.org/10.1016/j.matchemphys.2010.02.049.

[39] S. Alias, A. Ismail, A. Mohamad, Effect of pH on ZnO nanoparticle properties synthesized by sol–gel centrifugation, J. Alloy. Compd. vol. 499 (2) (2010) 231–237, https://doi.org/10.1016/j.jallcom.2010.03.174.

[40] G. Magesh, G. Bhoopathi, N. Nithya, A. Arun, E. Ranjith Kumar, Tuning effect of polysaccharide chitosan on structural, morphological, optical and photoluminescence properties of ZnO nanoparticles, Superlattices Microstruct. vol. 117 (2018) 36–45, https://doi.org/10.1016/j.spmi.2018.03.003.

[41] S. Senthilkumaar, K. Rajendran, S. Banerjee, T. Chini, V. Sengodan, Influence of Mn doping on the microstructure and optical property of ZnO, Mater. Sci. Semicond. Process. vol. 11 (1) (2008) 6–12, https://doi.org/10.1016/j.mssp.2008.04.005.

[42] S. Vorobyova, A. Lesnikovich, V. Muchinskii, Interphase synthesis and some characteristics of stable colloidal solution of CuO in octane, Colloids Surf. A: Physicochem. Eng. Asp. vol. 150 (1-3) (1999) 297–300, https://doi.org/10.1016/s0927-7757(98)00825-5.

[43] Y. Zheng, C. Chen, Y. Zhan, X. Lin, Q. Zheng, K. Wei, J. Zhu, Y. Zhu, Luminescence and photocatalytic activity of ZnO nanocrystals: correlation between structure and property, Inorg. Chem. vol. 46 (16) (2007) 6675–6682, https://doi.org/10.1021/ic062394m.

[44] M. Pereira, A. Silva-Neta, A. Farias, A. Souza, M. Fonseca, L. Pontes, I. Santos, Pure and Al-doped ZnO obtained by the modified Pechini method applied in ethanolic transesterification of cottonseed oil, Cerâmica vol. 63 (365) (2017) 82–89, https://doi.org/10.1590/0366-69132017633652066.

[45] Y. Song, S. Zhang, C. Zhang, Y. Yang, K. Lv, Raman spectra and microstructure of zinc oxide irradiated with swift heavy ion, Crystals vol. 9 (8) (2019) 395, https://doi.org/10.3390/cryst9080395.
[46] R. Berg, I. Ferré, S. Schäffer, Raman spectroscopy evidence of 1:1:1 complex formation during dissolution of WO_3 in a melt of $K_2S_2O_7$:K_2SO_4, Vib. Spectrosc. vol. 42 (2) (2006) 346–352, https://doi.org/10.1016/j.vibspec.2006.05.021.
[47] K. Sowri Babu, A. Ramachandra Reddy, K. Venugopal Reddy, Green emission from ZnO–MgO nanocomposite due to Mg diffusion at the interface, J. Lumin. vol. 158 (2015) 306–312, https://doi.org/10.1016/j.jlumin.2014.10.027.
[48] W. Sun, Y. Jia, R. Pang, H. Li, T. Ma, D. Li, J. Fu, S. Zhang, L. Jiang, C. Li, $Sr_9Mg_{1.5}(PO_4)_7$:Eu^{2+}: a novel broadband orange-yellow-emitting phosphor for blue light-excited warm white LEDs, ACS Appl. Mater. Interfaces vol. 7 (45) (2015) 25219–25226, https://doi.org/10.1021/acsami.5b06961.
[49] O.M. Ntwaeaborwa, S.J. Mofokeng, Vinod Kumar, R.E. Kroon, Structural, optical and photoluminescence properties of Eu^{3+} doped ZnO nanoparticles, Spectrochim. Acta Part A: Mol. Biomol. Spectrosc. vol. 182 (2017) 42–49, https://doi.org/10.1016/j.saa.2017.03.067.
[50] J. Dhanaraj, R. Jagannathan, T. Kutty, C. Lu, Photoluminescence characteristics of Y_2O_3:Eu^{3+} nanophosphors prepared using Sol−Gel thermolysis, J. Phys. Chem. B vol. 105 (45) (2001) 11098–11105, https://doi.org/10.1021/jp0119330.
[51] H. Sugimoto, K. Ebisawa, T. Okuno, Intense green luminescence from Eu^{2+}-doped ZnO microstructures, Jpn. J. Appl. Phys. vol. 46 (35) (2007) L839–L841, https://doi.org/10.1143/jjap.46.l839.
[52] W. Chen, J. Malm, V. Zwiller, Y. Huang, S. Liu, R. Wallenberg, J. Bovin, L. Samuelson, Energy structure and fluorescence of Eu^{2+} in ZnS:Eu nanoparticles, in: Physical Review B, vol. 61, 2000, pp. 11021–11024, https://doi.org/10.1103/physrevb.61.1102.
[53] T. Wanjun, H. Zhengxi, L. Jiaxuan, Controllable luminescence in Eu^{2+}-doped $Li_2Sr_2Al(PO_4)_3$ phosphor via tuning the Eu^{2+} concentration and codoping Ce^{3+}, J. Alloy. Compd. vol. 778 (2019) 612–617, https://doi.org/10.1016/j.jallcom.2018.11.204.
[54] V. Kumar, O. Ntwaeaborwa, T. Soga, V. Dutta, H. Swart, Rare earth doped zinc oxide nanophosphor powder: a future material for solid state lighting and solar cells, ACS Photonics vol. 4 (11) (2017) 2613–2637, https://doi.org/10.1021/acsphotonics.7b00777.
[55] Y. Liu, Y. Ding, Z. Peng, Q. Yu, X. Tian, G. Dong, Concentration quenching of Eu2+ in $Ba_2LiB_5O_{10}$:Eu^{2+} phosphor, Ceram. Int. vol. 40 (3) (2014) 5061–5066, https://doi.org/10.1016/j.ceramint.2013.09.026.
[56] Y. Kumar, A. Rana, P. Bhojane, M. Pusty, V. Bagwe, S. Sen, P. Shirage, Controlling of ZnO nanostructures by solute concentration and its effect on growth, structural and optical properties, Mater. Res. Express vol. 2 (10) (2015) 105017, https://doi.org/10.1088/2053-1591/2/10/105017.
[57] S. Shi, P. Wang, J. Cui, Z. Sun, Microstructure and doping/temperature-dependent photoluminescence of ZnO nano spears array prepared by hydrothermal method, Nanoscale Res. Lett. vol. 13 (1) (2018), https://doi.org/10.1186/s11671-018-2622-2.
[58] M. Cui, J. Wang, M. Shang, J. Li, Q. Wei, P. Dang, H. Jang, J. Lin, Full visible light emission in Eu^{2+}, Mn^{2+}-doped $Ca_9LiY_{0.667}(PO_4)_7$ phosphors based on multiple crystal lattice substitution and energy transfer for warm white LEDs with high colour-rendering, J. Mater. Chem. C. vol. 7 (12) (2019) 3644–3655, https://doi.org/10.1039/c9tc00109c.
[59] V. Mangalam, K. Pita, C. Couteau, Study of energy transfer mechanism from ZnO nanocrystals to Eu^{3+} ions, Nanoscale Res. Lett. vol. 11 (1) (2016), https://doi.org/10.1186/s11671-016-1282-3.
[60] C. He, H. Ji, Z. Huang, X. Zhang, Y. Liu, M. Fang, X. Wu, X. Min, Preparation, structure, luminescence properties of europium doped zinc spinel structure green-emitting phosphor $ZnAl_2O_4$:Eu^{2+}, J. Rare Earths vol. 36 (9) (2018) 931–938, https://doi.org/10.1016/j.jre.2018.01.018.
[61] Y. Liu, Y. Ding, Z. Peng, Q. Yu, X. Tian, G. Dong, Concentration quenching of Eu^{2+} in $Ba_2LiB_5O_{10}$:Eu^{2+} phosphor, Ceram. Int. vol. 40 (3) (2014) 5061–5066, https://doi.org/10.1016/j.ceramint.2013.09.026.
[62] S. Ma, W. Feng, R. Chen, Z. Peng, $KSr_4(BO_3)_3$:Pr^{3+}: A new red-emitting phosphor for blue-pumped white light-emitting diodes, J. Alloy. Compd. vol. 700 (2017) 49–53, https://doi.org/10.1016/j.jallcom.2017.01.069.
[63] Z. Yang, D. Xu, J. Sun, Synthesis and luminescence properties of $Ba_3Lu(PO_4)_3$:Sm^{3+} phosphor for white light-emitting diodes, Opt. Express vol. 25 (8) (2017) A391, https://doi.org/10.1364/oe.25.00a391.
[64] M. Zhang, J. Wang, W. Ding, Q. Zhang, Q. Su, A novel white light-emitting diode (w-LED) fabricated with $Sr_6BP_5O_{20}$:Eu^{2+} phosphor, Appl. Phys. B vol. 86 (4) (2006) 647–651, https://doi.org/10.1007/s00340-006-2535-0.